



## OPEN ACCESS

## EDITED BY

Tomoki Kurikawa,  
Future University Hakodate, Japan

## REVIEWED BY

Jannik Luboeinski,  
University Medical Center Göttingen,  
Germany  
Kanishk Chauhan,  
Stanford University, United States

## \*CORRESPONDENCE

M. Taher A. Saif  
✉ saif@illinois.edu

RECEIVED 01 November 2025

REVISED 20 January 2026

ACCEPTED 22 January 2026

PUBLISHED 11 February 2026

## CITATION

Lee KY and Saif MTA (2026) Tension shapes  
memory: computational insights into neural  
plasticity.

*Front. Comput. Neurosci.* 20:1737434.  
doi: 10.3389/fncom.2026.1737434

## COPYRIGHT

© 2026 Lee and Saif. This is an open-access  
article distributed under the terms of the  
[Creative Commons Attribution License  
\(CC BY\)](#). The use, distribution or reproduction  
in other forums is permitted, provided the  
original author(s) and the copyright owner(s)  
are credited and that the original publication  
in this journal is cited, in accordance with  
accepted academic practice. No use,  
distribution or reproduction is permitted  
which does not comply with these terms.

# Tension shapes memory: computational insights into neural plasticity

Ki Yun Lee<sup>1,2</sup> and M. Taher A. Saif<sup>1,2\*</sup>

<sup>1</sup>Department of Mechanical Science and Engineering, University of Illinois at Urbana-Champaign, Urbana, IL, United States, <sup>2</sup>Beckman Institute for Advanced Science and Technology, University of Illinois at Urbana-Champaign, Urbana, IL, United States

Mechanical forces have recently emerged as critical modulators of neural communication, yet their role in high-level cognitive functions remains poorly understood. Here, we present a biologically inspired spiking neural network model that integrates mechanical tension, vesicle dynamics, and spike-timing-dependent plasticity to examine how tension influences learning, memory, and cognitive operations such as pattern completion, projection, and association. We find that increased tension enhances synaptic efficiency by accelerating vesicle clustering and recovery, resulting in a 67% improvement in memory recall speed and a 17% increase in inter-regional synchrony during projection relative to relaxed states. Conversely, a 20% reduction in tension leads to a 31% decline in memory association performance, highlighting the tension-sensitive accessibility of stored information. The model further reveals that an appropriate balance of inhibition is essential for these tension-driven effects: networks with 20% inhibitory neurons achieve optimal spatial precision in memory encoding and recall, whereas insufficient inhibition allows tension-amplified excitation to spread uncontrollably and degrade recall fidelity. Together, these *in silico* findings position mechanical tension as a functional neuromodulator and suggest new directions for neuromorphic design and energy-efficient, living computing platforms.

## KEYWORDS

cognitive function, mechanical tension, memory, neural network, neuromodulation, synaptic plasticity

## Introduction

Neural communication is fundamental to high-level cognitive functions such as abstract thinking, decision-making, learning, and memory. Traditionally, these processes have been studied through chemical signaling mechanisms such as ion flux, neurotransmitter release, and receptor binding (Kandel et al., 2012; Kavalali, 2015). However, growing evidence suggests that mechanical forces, particularly tension arising from contractility of axons, also play a vital role in shaping neuronal behavior. The role of neuronal tension has been tested and verified by a wide range of experiments, both *in vitro* and *in vivo*. For instance, external forces can induce cytoskeletal remodeling and axonal outgrowth, processes central to neural plasticity (Dennerll et al., 1989; Pfister et al., 2004;

Siechen et al., 2009; Ahmed et al., 2012; Fan et al., 2015; Falconieri et al., 2023; Joy et al., 2023; Lee et al., 2023). Neurons generate and maintain contractile forces via the actomyosin cytoskeleton (Bray, 1979; Vogel and Sheetz, 2006; Tofangchi et al., 2016), and that tension increases during axon elongation and synapse formation. Notably, neurons may fail to function properly in the absence of tension, highlighting its importance not only for development, but also for ongoing neural activity, learning, and memory maintenance (Joy et al., 2023).

At the synaptic level, mechanical tension enhances vesicle clustering at presynaptic terminals, increases neural excitability, and promotes activity-dependent plasticity, that are strongly associated with enhanced synaptic efficacy. Experimental works with *Drosophila* embryos demonstrated that disrupting axonal tension reduced vesicle accumulation, while restoring tension recovered it (Siechen et al., 2009), and increasing tension further enhanced vesicle clustering (Ahmed et al., 2012; Figure 1A). *Ex vivo* mouse brain slices under cyclic stretch exhibited cumulative increases in excitability, suggesting the presence of a “mechanical memory” (Fan et al., 2015). Further, chemically modulating neural contractility altered vesicle accumulation, firing rates, and neural synchrony, reinforcing the idea that mechanical forces actively regulate neural signaling (Joy et al., 2023; Lee et al., 2023).

Mechanoneurobiology studies provide concrete protein dynamics underlying synaptic plasticity with tension: transmembrane proteins such as cadherins (Leckband and de Rooij, 2014) and integrins, particularly  $\beta 1$  and  $\beta 3$  subtypes (Calderwood et al., 2013), are mechanosensitive and transduce external or internally generated forces into biochemical signals. These studies have shown regulation of neural recognition and connectivity (Takeichi, 2007), synaptic formation and stabilization (Arikath, 2010), as well as synaptic density (Warren et al., 2012), strength (Pozo et al., 2012), and plasticity (Thalhammer and Cingolani, 2014). Motivated by this, we developed a computational model of a spiking neural network under mechanical tension, incorporating excitatory and inhibitory leaky integrate-and-fire neurons, vesicle dynamics, and synaptic plasticity. We hypothesize that mechanical tension enhances synaptic strength and facilitates cognitive functions by increasing vesicle availability and modulating network dynamics.

A neural assembly refers to a group of interconnected neurons that tend to activate together within a network, forming functionally meaningful units (Attneave and Hebb, 1950; Gerstein et al., 1989; Langille and Brown, 2018). According to Hebbian theory, neurons within an assembly respond collectively to stimuli rather than acting independently (Attneave and Hebb, 1950). To model such behavior at a higher level of abstraction, a framework known as assembly calculus was developed (Papadimitriou et al., 2020). This framework enables simulation of cognitive operations such as pattern completion (retrieving a full pattern from partial input), projection (forming a new assembly via activation of an existing one), and association (linking two assemblies such that activation of one triggers the other). Assembly calculus introduces control over network activation using parameters such as the total number of neurons ( $n$ ) and the maximum number of simultaneously spiking neurons ( $k$ ), with  $k$  effectively simulating inhibition by restricting widespread activation. While this symbolic approach enables computational modeling of high-level operations, it abstracts away the underlying biophysical mechanisms. In

contrast, our model implements these cognitive functions within a biophysically realistic framework, capturing the dynamics of individual neurons, synapses, and vesicle clustering. This allows us to examine how cognitive operations might emerge from low-level, biologically grounded neural and synaptic interactions.

Hebbian theory posits that learning and memory arise from activity-dependent changes in synaptic plasticity, such as synaptogenesis and adjustments in synaptic weight, leading to the formation of neural assemblies that can support cognitive operations (Attneave and Hebb, 1950). Repeated stimulation of neurons (i.e., learning) strengthens their synaptic connections, allowing assemblies to temporarily operate as functional units that can later be reactivated (Gerstein et al., 1989). However, a key limitation of Hebbian learning is the unbounded growth of synaptic weights, which can destabilize the network by causing assemblies to merge into the broader network. Oja’s rule was introduced as an early solution to this problem by incorporating a normalization term that constrains synaptic weights (Oja, 1982).

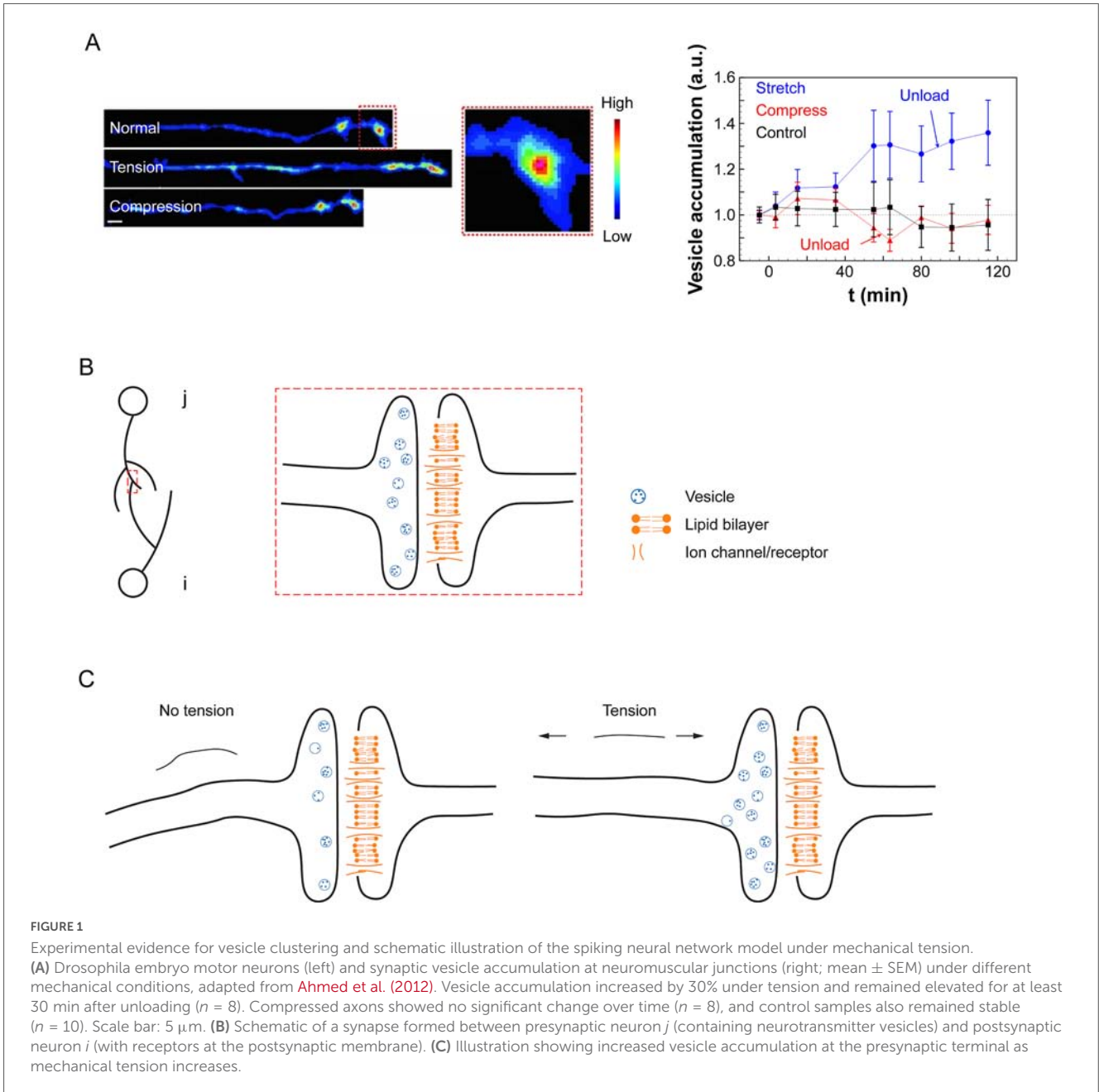
In our model, rather than implementing Oja’s rule directly, we address this limitation using spike-timing-dependent plasticity (STDP) combined with a biologically motivated forgetting mechanism supported by experimental evidence. Such experiments include reduced reactivation of the original engram ensemble and decreased spine density in engram cells (O’Leary et al., 2024), as well as transitions of engrams from accessible to inaccessible states mediated by circuit-level and plasticity changes (Ryan and Frankland, 2022). Inspired by these observations, our implementation of forgetting constrains unbounded synaptic growth while preserving activity-dependent learning. This balance enables the formation and selective reactivation of neural assemblies without destabilizing overall network dynamics.

We further incorporate mechanical tension as a dynamic variable to probe its role as a neuromodulator. Using a biologically inspired spiking neural network composed of excitatory and inhibitory neurons, and integrating learning-based synaptic plasticity with vesicle dynamics, we examined how training duration and tension level, and inhibition influence pattern completion, memory encoding and recall, and the emergence of higher-order cognitive operations such as projection and association. Our simulations demonstrate successful pattern completion, projection, and associative memory recall following training, indicating functional plasticity in the trained network. These results suggest that mechanical tension shapes the dynamics of neural assemblies, influencing not only firing and plasticity but also inter-assembly interactions.

## Materials and methods

### Spiking neural network model

We constructed a spiking neural network comprising 4,000 excitatory and 1,000 inhibitory neurons randomly distributed within a bounded 2D space. The 4:1 excitatory-to-inhibitory ratio was chosen based on physiological data from the rodent hippocampus (Gulyás et al., 1999; Bezaire and Soltesz, 2013) and primate cortex (Hendry et al., 1987; DeFelipe et al., 2002), as well as prior simulation studies (Brunel, 2000; Kriener et al., 2014).



Each neuron was assigned multiple neurites (dendrites and axons), with lengths drawn from a normal distribution (mean = 200  $\mu\text{m}$ ; standard deviation = 40  $\mu\text{m}$ ). A potential connection was considered only if the combined neurite lengths of two neurons exceeded the distance between them; for these eligible pairs, a synapse was formed with a probability of 0.1. Self-connections were not permitted, and each presynaptic neuron could form at most one synapse with any given postsynaptic neuron.

### Neural communication dynamics

We modeled synaptic transmission between a presynaptic neuron  $j$  and a postsynaptic neuron  $i$  (Figure 1B; Equation 1). The presynaptic neuron clusters neurotransmitter-filled vesicles at its terminal, while the postsynaptic neuron clusters neurotransmitter receptors at the synaptic membrane. The membrane potential of

neuron  $i$  at time  $t$ , denoted as  $V_i(t)$ , is initialized at a resting potential  $V_{rest}$  in the absence of stimulation.

When an action potential (AP) arrives at the presynaptic terminal of neuron  $j$ , neurotransmitters are released and they bind to receptors on neuron  $i$ , inducing ion flux and increasing  $V_i(t)$  by an amount  $V_{synapse}(t)$ . If  $V_i(t)$  exceeds the firing threshold  $V_{threshold}$ , the neuron generates a spike. After firing,  $V_i(t)$  decays exponentially with membrane time constant  $\tau_{membrane}$ . Let  $t_j^m$  and  $t_i^n$  represent the  $m$ -th and  $n$ -th spike times of neurons  $j$  and  $i$ , respectively.

The synaptic potential  $V_{synapse}(t)$  depends on the spike timing history of the pre- and postsynaptic neurons. When neuron  $j$  fires shortly before neuron  $i$  ( $t_j^m < t_i^n$ ), the synapse is potentiated; if the firing order is reversed, the synapse is weakened. The magnitude of synaptic plasticity is modulated by the time difference between spikes, following a STDP rule.

The model also includes an external input term  $V_{external}(t)$  to account for depolarization due to defined stimuli (e.g., electrical or optogenetic) or stochastic influences (e.g., chemical neuromodulators or glial interactions) (Song et al., 2000; Kriener et al., 2014). Stochastic activity is simulated using a Poisson process, where a randomly selected subset of neurons ( $N_{external}$ ) generates spikes with interspike intervals (ISI) drawn from an exponential distribution with mean  $r_{external}$ . The membrane potential  $V_i(t)$  evolves according to the leaky integrate-and-fire (LIF) model (van Vreeswijk and Sompolinsky, 1996; Brunel, 2000; Kriener et al., 2014).

$$\tau_{membrane} \frac{dV_i(t)}{dt} = -V_i(t) + V_{rest} + V_{synapse}(t) + V_{external}(t) \tag{1}$$

$$V_i(0) = V_{rest}$$

### Synaptic potential, $V_{synapse}(t)$

The synaptic input  $V_{synapse}(t)$  received by postsynaptic neuron  $i$  is composed of two terms: a default potential  $J_{ji}(t)$ , representing baseline vesicle release, and a history-dependent term  $s(t)w_{ji}(t)$ , shaped by spike timing and synaptic plasticity (Equation 2). Both components are modulated by mechanical tension. This additive formulation reflects the biophysical principle that postsynaptic membrane potentials arise from the linear summation of independent synaptic and intrinsic currents at subthreshold voltages. Separating baseline input from history-dependent synaptic potentials allows their respective contributions to neural transmission to be independently modulated and interpreted in response to mechanical tension and prior activity. The total synaptic potential is given by:

$$V_{synapse}(t) = \begin{cases} \sum_j (J_{ji}(t) + s(t)w_{ji}(t)) \delta(t - t_j^m), & \text{from excitatory} \\ -\gamma \sum_j (J_{ji}(t) + s(t)w_{ji}(t)) \delta(t - t_j^m), & \text{from inhibitory} \end{cases} \tag{2}$$

The Dirac delta function  $\delta(x)$  has the property of approaching  $\infty$  when  $x = 0$ , equaling 0 otherwise, and satisfying the identity  $\int_{-\Delta x}^{\Delta x} \delta(x) dx = 1$ . Consequently, when the synaptic potential (Equation 1) is integrated with respect to time from 0 to  $t$ ,  $V_{synapse}(t)$  contributes discrete, finite increases to the membrane potential  $V_i(t)$  at each spike time  $t_j^m$  of presynaptic neuron  $j$  (where  $j = 1, 2, \dots$ , and  $m$  denotes the spike index).

The sign of  $V_{synapse}(t)$  depends on whether the presynaptic neuron is excitatory or inhibitory, determined by the type of neurotransmitter released, typically glutamate for excitatory neurons and GABA for inhibitory neurons (Brunel, 2000; Kriener et al., 2014). The parameter  $\gamma$  denotes the ratio of excitatory to inhibitory neurons in the network and influences the overall excitability and balance of the system.

### History-independent component of $V_{synapse}$ , $J_{ji}(t)$

The term  $J_{ji}(t)$  represents the default synaptic potential generated by the release of a baseline number of vesicles (Equation 3). This component is independent of the synaptic firing history but depends on the presynaptic vesicle clustering capacity, which is influenced by mechanical tension. As vesicle accumulation

increases under higher tension (Siechen et al., 2009; Ahmed et al., 2012; Lee et al., 2023), we model  $J_{ji}(t)$  as a function of network-wide mechanical tension (Figure 1C).

$$J_{ji}(t) = J + c_1 \left( 1 - e^{-c_2 \frac{\epsilon(t) - \epsilon_0}{\epsilon_0}} \right) \tag{3}$$

Here,  $c_1$ ,  $c_2$ , and  $J$  are constants. The term  $J$  represents the baseline synaptic potential resulting from vesicle release under a uniform resting tension, denoted as  $\epsilon_0$ , applied across the entire network. When the mechanical tension increases to  $\epsilon(t)$ , vesicle clustering at the presynaptic terminal is enhanced. This increased vesicle capacity leads to a potentiation of  $J_{ji}(t)$ , thereby amplifying the synaptic input in a tension-dependent manner.

### History-dependent component of $V_{synapse}$ , $s(t)w_{ji}(t)$

The product  $s(t)w_{ji}(t)$  represents the plastic, history-dependent component of synaptic transmission. Here,  $s(t)$  denotes the expected volume of neurotransmitter vesicles released from presynaptic neuron  $j$  upon firing at time  $t$ , calculated as the product of vesicle release probability  $u(t)$  and vesicle availability  $R(t)$  at the presynaptic terminal. The synaptic weight  $w_{ji}(t)$  represents the change in postsynaptic membrane potential per unit volume of released vesicles. Together, this product quantifies the effective contribution to the membrane potential  $V_i(t)$  in response to an action potential from neuron  $j$ .

### Vesicle release probability, $u(t)$

Let  $u(0) = u_0$  denote the baseline probability of vesicle release in the absence of recent synaptic activity (Figure 2A; Equation 4). Upon presynaptic firing,  $u(t)$  increases due to  $Ca^{2+}$  influx at the presynaptic terminal, a well-documented mechanism in neurotransmitter release (Bertram et al., 1996; Tsodyks et al., 1998). This increase is transient and decays back toward the baseline  $u_0$  as intracellular  $Ca^{2+}$  is resorbed, with a time constant  $\tau_u$ . The increment in  $u(t)$  depends on its value at the moment of presynaptic firing, denoted by  $u(t_j^m)$ , where  $t_j^m$  is the  $m$ -th spike time of neuron  $j$ . Since the probability is bounded between  $u_0$  and 1, the dynamics of  $u(t)$  is modeled as:

$$\tau_u \frac{du(t)}{dt} = -u(t) + u_0 + u_0(1 - u(t)) \delta(t - t_j^m) \tag{4}$$

$$u(0) = u_0$$

$$u(t_j^{m+}) = u(t_j^m) + u_0(1 - u(t_j^m))$$

For instance, if neuron  $j$  fires for the first time at  $t = t_j^1$ , then  $u(t_j^1) = u_0$ , and immediately after firing,  $u(t_j^{1+}) = u(t_j^1) + u_0[1 - u(t_j^1)] = u_0 + u_0(1 - u_0) = 2u_0 - u_0^2$ . Following this spike-induced increase,  $u(t)$  decays exponentially back to  $u_0$  in the absence of further firing with a time constant of  $\tau_u$ .

### Vesicle availability, $R(t)$

When presynaptic neuron  $j$  fires for the  $m$ -th time at  $t = t_j^m$ , it begins with a default vesicle volume  $R_0$  available for release (Equations 5, 6). Immediately after firing at  $t = t_j^{m+}$ , the vesicle

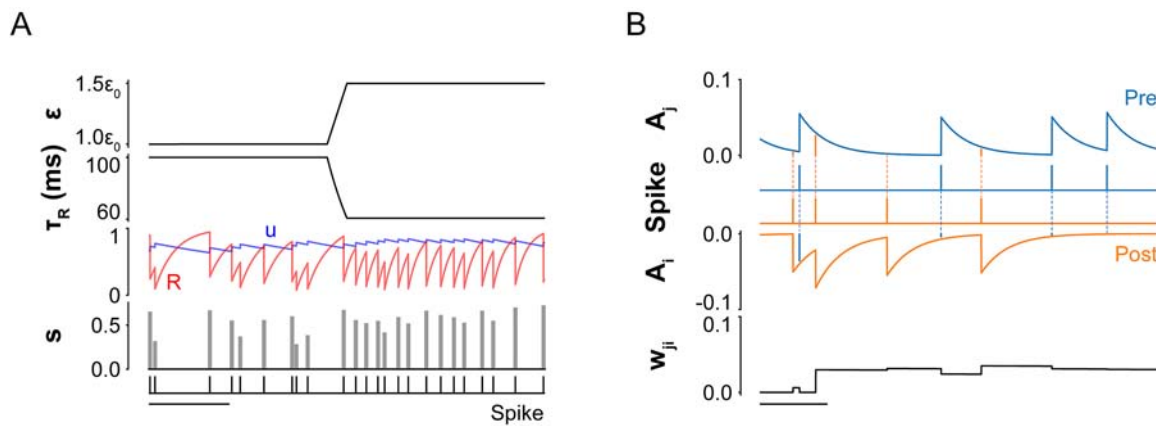


FIGURE 2

Dynamics of synaptic variables modulated by mechanical tension. (A) Vesicle-related dynamics under different tension levels ( $\epsilon$ ). Time course plots show four key variables: vesicle recovery time constant ( $\tau_R$ ), release probability ( $u$ ), vesicle availability ( $R$ ), and expected volume of vesicles released ( $s$ ). After a presynaptic neuron fires,  $u$  increases due to  $\text{Ca}^{2+}$  influx and then decays exponentially back to its baseline ( $u_0$ ) in the absence of further activity. Simultaneously,  $R$  decreases as vesicles are released, then recovers toward baseline with time constant  $\tau_R$ . The expected vesicle release volume,  $s$ , is defined as the product  $u \times R$ . Increased tension reduces  $\tau_R$ , thereby accelerating vesicle replenishment and enabling greater vesicle output ( $s$ ) during subsequent spikes (see Materials and methods: Table 1. All parameters used in simulation for details of parameters). Scale bar: 400 ms. (B) Time evolution of history-dependent synaptic weight ( $w_{ji}$ ). Synaptic weight dynamics are shaped by the relative spike timings of the presynaptic neuron  $j$  and the postsynaptic neuron  $i$ . Each neuron has a spike trace variable ( $A_j$  for the presynaptic and  $A_i$  for the postsynaptic neuron) that updates with each spike:  $A_j$  increases upon a presynaptic spike and decays back to zero, while  $A_i$  decreases upon a postsynaptic spike and also decays to zero over time.  $w_{ji}$  increases by  $A_j(t_j)$  when the postsynaptic neuron fires and decreases by  $A_i(t_j)$  when the presynaptic neuron fires. The magnitude of these changes is modulated by the temporal proximity of the spikes: shorter intervals lead to stronger potentiation or depression.  $w_{ji}$  is bounded between 0 and a maximum value,  $w_{max}$ . Scale bar: 50 ms.

pool is depleted proportionally to the release probability, such that  $R(t_j^{m+}) = R(t_j^m) - u(t_j^{m+})R(t_j^m)$ . The dynamics of  $R(t)$  is given by:

$$\tau_R(t) \frac{dR(t)}{dt} = -R(t) + R_0 - u(t)R(t)\delta(t - t_j^m) \quad (5)$$

$$R(0) = R_0$$

$$R(t_j^{m+}) = R(t_j^m) - u(t_j^{m+})R(t_j^m)$$

$$\tau_R(\epsilon) = \tau_0 e^{-\frac{\epsilon - \epsilon_0}{\epsilon_0}} \quad (6)$$

Following this depletion, the vesicle reserve  $R(t)$  recovers over time with a recovery time constant  $\tau_R(\epsilon)$ . This recovery is tension-dependent: as mechanical tension  $\epsilon(t)$  increases, the recovery becomes faster, that is  $\tau_R(\epsilon)$  decreases relative to the baseline  $\tau_0$ .

Lastly, expected volume of released vesicles,  $s(t)$  is defined as follows (Equation 7):

$$s(t_j^m) = u(t_j^{m+})R(t_j^m) \quad (7)$$

### Synaptic weight, $w_{ji}(t)$

The synaptic weight  $w_{ji}(t)$  represents the postsynaptic potential change per unit volume of neurotransmitter vesicles released by presynaptic neuron  $j$  (Figure 2B; Equations 8-10). In line with Hebbian theory, we modeled learning-induced plasticity using a STDP framework (Song et al., 2000; Morrison et al., 2008; Gerstner et al., 2014), which is strongly supported by experimental evidence in hippocampal and cortical neurons (Magee and Johnston, 1997; Markram et al., 1997; Bi and Poo, 1998; Feldman, 2000).

Synaptic weights are updated based on the relative timing of spikes from presynaptic neuron  $j$  and postsynaptic neuron  $i$ . When  $j$  fires shortly before  $i$  (i.e.,  $t_j^m < t_i^n$ ),  $w_{ji}(t)$  increases, reflecting the strengthening of the synapse. Conversely, when  $j$  fires after  $i$  ( $t_j^m > t_i^n$ ), the synapse is weakened, and  $w_{ji}(t)$  decreases. These updates can be reasoned as follows. When presynaptic firing precedes postsynaptic activation, neurotransmitter binding at the postsynaptic terminal facilitates depolarization and increases synaptic efficacy. In contrast, postsynaptic firing before presynaptic input can trigger back-propagating action potentials and local  $\text{Ca}^{2+}$  influx through NMDA receptors, leading to attenuation in synaptic potential (Bliss and Collingridge, 1993; Magee and Johnston, 1997; Markram et al., 1997). The amount of change in  $w_{ji}(t)$  depends on the time difference between firing times,  $t_j^m$  and  $t_i^n$ , the shorter the time difference, the higher the change.

To implement this in the model, we introduced two temporal traces of pre and postsynaptic neuron:  $A_j(t)$  and  $A_i(t)$ . When neuron  $j$  fires at  $t = t_j^m$ ,  $A_j(t)$  is incremented by a fixed amount  $F_w$  and then decays exponentially with a time constant  $\tau_w$ . Similarly, when neuron  $i$  fires at  $t = t_i^n$ ,  $A_i(t)$  drops sharply and also increases with the same time constant.

$$\tau_w \frac{dA_j(t)}{dt} = -A_j(t) + F_w \delta(t - t_j^m) \quad (8)$$

$$A_j(0) = 0$$

$$\tau_w \frac{dA_i(t)}{dt} = -A_i(t) - F_w \delta(t - t_i^n) \quad (9)$$

$$A_i(0) = 0$$

$$\Delta w_{ji}(t) = \begin{cases} A_j(t), & \text{at } t = t_i^m \\ A_i(t), & \text{at } t = t_j^m \end{cases} \quad (10)$$

Finally, to prevent unbounded growth,  $w_{ji}(t)$  decays continuously over time with a forgetting rate  $\alpha$  and  $w_{ji}(t)$  is bounded within the range  $[0, w_{max}]$  (Equation 11).  $w_{ji}(t)$  was initialized to zero, meaning that at the beginning of the simulation there is no effective synaptic transmission between neurons. While this initialization is a modeling simplification, it is qualitatively consistent with our experimental observations from mouse hippocampal neuron cultures grown on microelectrode arrays (data not shown). In such systems, neurons exhibit isolated, spontaneous spiking during early developmental stages ( $\sim$  day 6), with little to no coordinated network activity or propagation to neighboring neurons. Robust network-level transmission typically emerges only after several days (after day 8) *in vitro*, coinciding with synaptogenesis and strengthening of synaptic connections. Although the timescales differ between *in vitro* experiments and simulations in our model, this developmental progression is compressed in time and represented by the transition from zero initial synaptic weights to strengthened connections through STDP.

$$\frac{dw_{ji}(t)}{dt} = -\alpha w_{ji}(t) \quad (11)$$

$$w_{ji}(0) = 0$$

All model parameters are summarized in Table 1.

## In silico stimulation

*In silico* stimulation was implemented as repeated single-pulse stimuli delivered at 50 Hz during the training phase and 10 Hz during the recall phase for stimulation time step (0.1 ms), applied to predefined regions of the simulated neural network. Each stimulation pulse induced an instantaneous increase of 2 mV in the membrane potential of stimulated neurons. Mechanical tension was modulated during the recall phase to assess its effect on memory retrieval dynamics. All simulations were conducted in Python (v3.10.13) using standard scientific libraries and previously published neural models (Gerstner et al., 2014; Stimberg et al., 2019; Gillies et al., 2022).

## Synchrony index between two assemblies

Assembly activity was defined as a period of highly correlated, fast spiking from neurons within a single assembly, characterized by interspike intervals (ISIs) shorter than 0.5 ms. The duration of an assembly activity extended from the onset of the earliest spike to the offset of the latest spike. If an additional neuron fired within 0.5 ms of the most recent spike in the activity, the duration was extended to include that spike. In addition, the instantaneous spike rate at the center of the activity was required to exceed 100 Hz. These criteria were chosen to isolate high-frequency spiking events potentially

analogous to ripple oscillations observed *in vivo* and *in vitro*, which are implicated in memory-related neural processes (Jadhav et al., 2012; Buzsáki, 2015; Norman et al., 2019).

The synchrony index quantifies the temporal coordination between two neural assemblies: a cue-stimulated assembly and a second assembly that was co-trained during the training phase through simultaneous patterned stimulation of both regions, but was not directly stimulated during the recall phase. During training, both assemblies were activated concurrently (co-trained), allowing synaptic associations to form between them. To compute the index, assembly activities from both assemblies were vectorized across all detected events. The synchrony index ( $\chi$ ) between two activity vectors,  $x$  and  $y$ , was calculated using normalized cross-correlation as follows.

$$\chi = \frac{\sum x_i y_i}{\sqrt{\sum x_i^2 \cdot \sum y_i^2}}$$

$x_i$  and  $y_i$  are the  $i$ -th elements of the respective vectors. A value of  $\chi = 1$  indicates perfect synchrony, while  $\chi = 0$  indicates complete asynchrony. Note that  $x_i$  or  $y_i$  can have values of either 0 or 1.

## Clustering of spiking neurons and intersection over union

To quantify the spatial spread of spiking neurons following stimulation, we applied the density-based spatial clustering of applications with noise (DBSCAN) algorithm (Ester et al., 1996) over a 5 ms analysis window. DBSCAN identifies clusters by locating core points within dense regions of spiking activity in 2D space and expands each cluster by including neighboring points within a defined radius. A spiking neuron was considered part of a cluster if it met the following DBSCAN parameters:

- Maximum distance between two neurons: 120  $\mu\text{m}$ ;
- Minimum number of neighboring neurons to form a core point: 20.

Once clusters were identified, we computed the spatial similarity between the leaked area ( $A_{leak}$ , the area covered by the resulting spiking neuron cluster within 5 ms after cue) and the trained area ( $A_{train}$ ) using the intersection over union (IoU) metric:

$$IoU = \frac{A_{train} \cap A_{leak}}{A_{train} \cup A_{leak}}$$

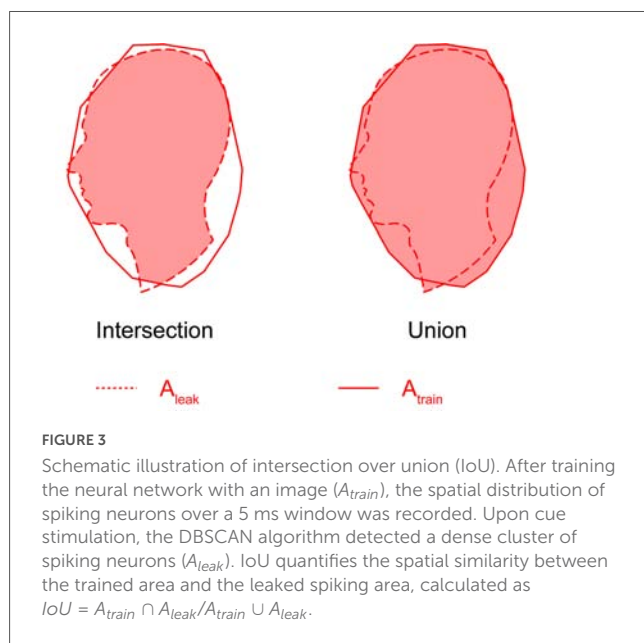
The intersection and union are calculated as the overlapping area and the total combined area of  $A_{train}$  and  $A_{leak}$ , respectively (Figure 3). An IoU of 1 indicates perfect spatial overlap between the activated and trained regions, while lower values indicate greater spatial divergence.

## Statistical analysis

Statistical analyses were performed using Python and associated scientific libraries (Vallat, 2018). All data are reported as

TABLE 1 All parameters used in simulation.

Abbreviation	Value	Description	Abbreviation	Value	Description
$dt$	0.1 ms	Simulation time step	$V_{rest}$	-74 mV	Resting potential
$V_{reset}$	-60 mV	Reset potential	$V_{threshold}$	-54 mV	Firing threshold
$\tau_{membrane}$	10 ms	Membrane time constant			
$N_{external}$	1,000	Number of external neurons in the Poisson point process	$\tau_{external}$	13 Hz	Average interval of spikes in the Poisson point process
$J$	0.01 mV	Vesicle release at resting tension	$\epsilon_0$	0.001	Resting tension
$c_1$	0.1 mV	Constant (Equation 3)	$c_2$	0.01	Constant (Equation 3)
$u_0$	0.2	Initial vesicle release probability	$\tau_u$	1,000 ms	Vesicle release probability time constant
$R_0$	1	Initial volume of available vesicles	$\tau_0$	100 ms	Vesicle recovery time constant at resting tension
$\alpha$	0.25 Hz	Forgetting rate	$w_{max}$	5	Maximum synaptic weight
$\tau_w$	20 ms	Spike trace time constant	$F_w$	0.05	Spike trace amplitude



mean  $\pm$  standard error of the mean (SEM), with  $n$  denoting the number of biological or simulated replicates. Statistical significance was set at  $p < 0.05$ , and significance levels are indicated as follows:  $p < 0.05$  (\*),  $p < 0.01$  (\*\*), and  $p < 0.001$  (\*\*\*). Normality was assessed using skewness and kurtosis thresholds ( $|\text{skewness}| < 1$ ;  $|\text{kurtosis}| < 2$ ), and power transformations were applied to non-normal data to meet these criteria.

Activation time in the pattern completion task and the synchrony index in the projection task were analyzed using one-way ANOVA. Intersection-over-union (IoU) values were evaluated using two-way ANOVA, with the proportion of inhibitory neurons and memory phase (encoding vs. recall) as between-subject factors. Synchrony index in the association task was analyzed using repeated-measures two-way ANOVA, with recall time as the within-subject factor and training duration as the between-subject factor. Post hoc comparisons

were conducted using Tukey's honestly significant difference (HSD) test.  $F$  statistics are reported in the form  $F_{m,n}$ , where  $m$  and  $n$  represent the degrees of freedom between and within groups, respectively.

## Results

### Training duration and tension enhance pattern completion

The network consisted of 4,000 excitatory and 1,000 inhibitory neurons, forming both excitatory and inhibitory synapses (Figure 4A). A face-shaped region within the network was selectively trained to encode an input pattern. Following training, localized rectangular cues were delivered within this trained region to evaluate whether partial input could elicit recall of the embedded memory via activation of the neural assembly. The total area of the rectangular cues covered 20% of the trained region.

During training, neurons within the face-shaped region responded to the stimuli and fired in a coordinated manner (Figure 4B). In the recall phase, neurons within the cue regions activated in response to the stimuli, and this activity rapidly propagated across the trained area within 10 ms. This spread was driven by the elevated synaptic weights acquired during training. Notably, the activity remained spatially confined to the trained region, as synaptic weights outside this area were insufficient to trigger widespread firing, consistent with localized pattern completion. In contrast, the untrained network showed no propagation beyond the cue site, confirming that training was required for memory-like recall behavior. Dynamic propagation of spikes in both trained and untrained networks is visualized in [Supplementary Video S1](#).

To visualize rapid assembly activation immediately following cue stimulation, we compared average population activity in the trained and untrained regions (Figure 4C). Spike rates were computed as population firing rates by counting the total number of spiking neurons within each region in

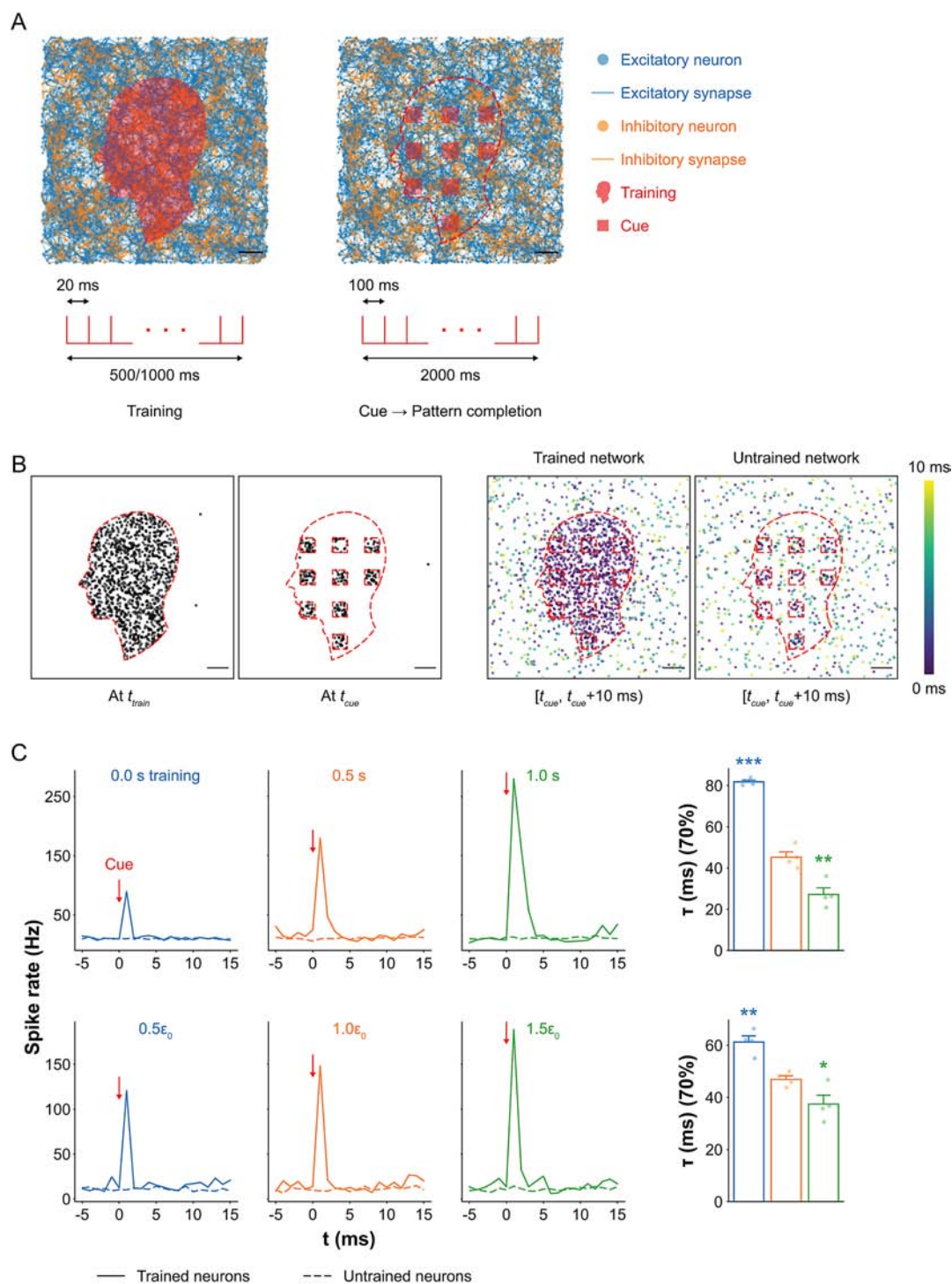


FIGURE 4

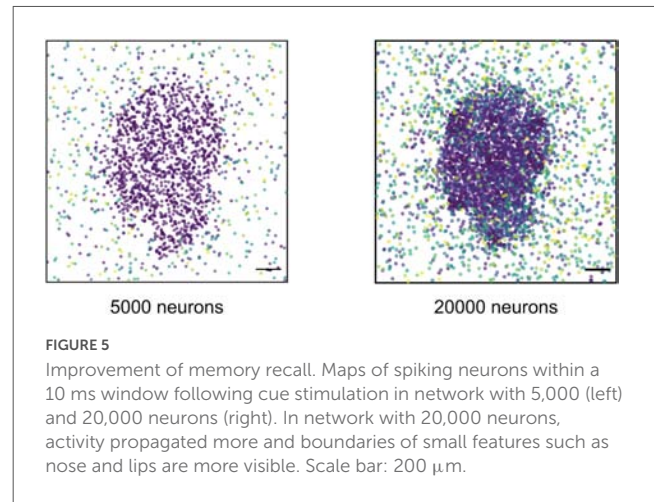
Pattern completion *in silico* under mechanical tension. **(A)** Visualization of spiking neural networks (top) and corresponding stimulation protocols (bottom) during training and recall. During training, neurons within a face-shaped region were repeatedly stimulated. For recall, rectangular subregions covering 20% of the trained area were partially stimulated to assess memory recall. Scale bar: 200  $\mu$ m. **(B)** Maps of spiking neurons during training and recall (left), and spiking activity within a 10 ms window following cue stimulation in trained and untrained networks (right). In trained networks, activity propagated from the cue sites across the trained region, while neurons outside the trained area exhibited only spontaneous firing. In contrast, untrained networks showed localized activity restricted to the cue sites, with no propagation. Scale bar: 200  $\mu$ m. **(C)** Average spike rates in trained vs. untrained regions as a function of training duration (top) and tension level (bottom). Activation times to reach 70% firing in the trained assembly are shown for each condition (right; mean  $\pm$  SEM;  $n = 4$ ). In the 0.5 s training condition, neurons in the trained region exhibited a sharp spike in activity upon cue stimulation, while neurons in the untrained region showed no change, indicating precise pattern completion. Networks with no training showed a 50% lower peak spike rate, with only a small bump caused by direct activation at the cue site. Longer training (1 s) led to a 56% increase in peak spike rate and sustained firing, along with a 40% reduction in activation time compared to 0.5 s training. Conversely, untrained networks had 81% longer activation times. Increased mechanical tension raised the peak spike rate by 27% and shortened activation time by 20%, while relaxation reduced spike rates by 19% and increased activation time by 31%. Significance levels are shown relative to 0.5 s training or baseline tension (0.1%). Significance levels are indicated as follows: \* $p < 0.05$ , \*\* $p < 0.01$ , and \*\*\* $p < 0.001$ .

successive 1 ms time windows and normalized to the number of neurons in the region of interest. In the 0.5 s training condition, spike rates in the trained region exhibited a sharp increase within 5 ms of cue onset and then decayed rapidly, while spike rates in the untrained region remained low and stable. This indicates that memory-related activity was confined to the trained assembly. The 1 s training condition produced a peak spike rate 56% higher than that of the 0.5 s condition, demonstrating that extended training enhances pattern completion. In contrast, the untrained network showed only a transient spike at the cue site (peak  $\approx 89$  Hz), followed by rapid decay, reflecting a lack of propagation due to weak synaptic connectivity.

We also measured activation time, defined as the time required for 70% of neurons within the trained region to become active following the cue. Activation time decreased by 40% when training duration increased from 0.5 s to 1 s ( $p = 0.0049$ ), reflecting faster recruitment due to strengthened synaptic connectivity within the trained assembly and consequently more rapid activity spread. In contrast, activation time increased by 81% in the untrained network compared to the trained network for 0.5 s ( $p < 0.001$ ; one-way ANOVA,  $F_{2,9} = 129.86$ ,  $p < 0.001$ ). This increase arises because the untrained network lacks reinforced recurrent connections. Therefore, cue-evoked activity relies solely on weak baseline connectivity and propagates more slowly. Together, these results further support that training duration enhances the speed of memory recall.

We next investigated how mechanical tension during recall modulates memory retrieval. Compared to the baseline tension condition, a 50% reduction in network tension resulted in a 19% decrease in spike rate, while a 50% increase in tension enhanced spike rate by 27%. Activation time mirrored these effects: networks under higher tension recalled the pattern 20% faster ( $p = 0.0407$ ), while networks under lower tension recalled 31% more slowly ( $p = 0.0018$ ; one-way ANOVA,  $F_{2,9} = 22.94$ ,  $p < 0.001$ ). These findings suggest that mechanical tension modulates synaptic efficiency, likely through its influence on vesicle availability and recovery dynamics.

Lastly, to assess the role of representational resolution independent of mechanical tension, we investigated whether increasing network size alone could improve the precision of memory recall, particularly the representation of fine facial features such as the nose and lips. To this end, we increased the total number of neurons fourfold to 20,000, resulting in a cell density of 5,000 cells/mm<sup>2</sup>, comparable to previous *in vitro* experiments (Joy et al., 2023; Lee et al., 2023) and to estimated neural densities in the human hippocampus, assuming a tissue thickness of 0.25–0.3 mm (Furcila et al., 2019). The expanded network was trained and cued using the same protocol as before. Spiking activity maps revealed that the 20,000-neuron network reproduced the face pattern better than the 5,000-neuron network (Figure 5), with finer features such as the nose and lips more clearly represented. These results suggest that even a relatively simple model, compared to the highly intricate architecture of the human brain, can exhibit improved memory recall performance with increased neural density.



## Inhibitory neurons are critical for memory encoding and recall

In addition to examining the effects of mechanical tension on learning and memory, we investigated how the balance between excitatory and inhibitory neurons modulates memory formation and retrieval in the network. To this end, we constructed networks with varying ratios of inhibitory to excitatory neurons and trained each for 1 s. Memory encoding and recall were assessed by analyzing the spatial spread of spiking activity following training and cue application. Spiking neurons were recorded over a 5 ms window, and cluster size was quantified using DBSCAN (see Materials and methods: clustering of spiking neurons and intersection over union for details).

During encoding, networks without inhibitory neurons (0%) exhibited widespread spiking beyond the trained region,  $A_{train}$ , producing a larger activation area,  $A_{leak}$  (Figure 6A). This resulted from unregulated excitation, as all presynaptic inputs were excitatory. As inhibitory neurons were introduced,  $A_{leak}$  became more confined to  $A_{train}$ , because inhibitory inputs reduced postsynaptic membrane potentials and suppressed neural transmission, effectively sharpening the spatial boundary of activity. In the 100% inhibitory condition, spiking was tightly localized, effectively embedding the stimulus pattern while sharply constraining spread. Thus, in terms of encoding fidelity, networks with more inhibition formed sharper, more well-defined memory traces.

However, recall revealed a different pattern. In 0% inhibitory networks, the cue-induced activity spread uncontrollably, resulting in diffuse and imprecise activation that extended far beyond  $A_{train}$  (Figure 6B). In contrast, 100% inhibitory networks showed minimal activity beyond the cue site, suggesting a failure to retrieve the full embedded pattern despite successful encoding. Notably, networks with 20% inhibitory neurons achieved both containment and propagation of activity, accurately recalling the stored pattern with high spatial precision.

These patterns were also reflected in spike rate measurements during recall (Figure 6C). Networks without inhibition (0%) showed the highest spike rates, reflecting runaway excitation. In contrast, fully inhibitory (100%) networks showed a minimal

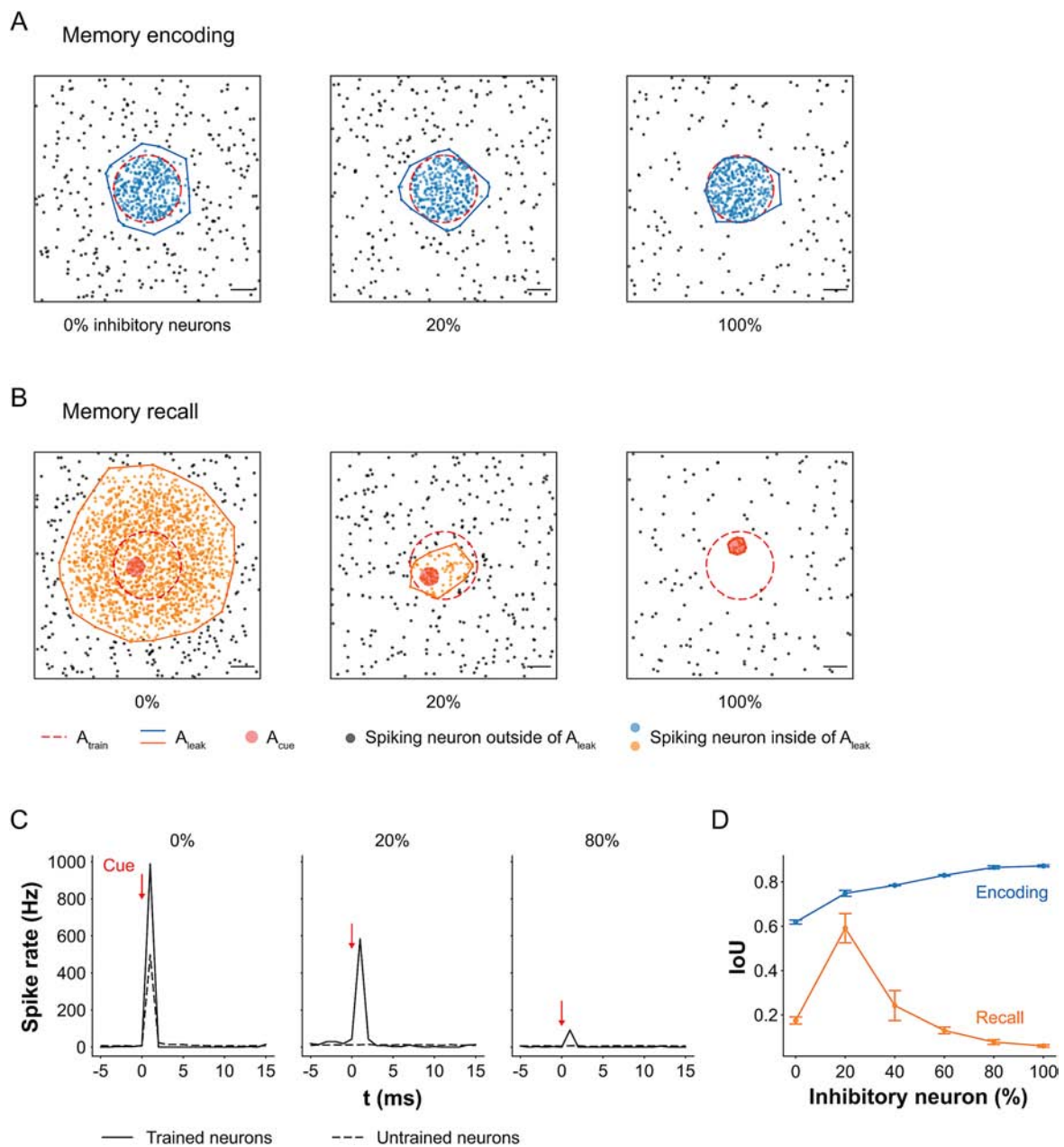


FIGURE 6

Role of inhibitory neurons in memory encoding and recall. **(A)** Maps of spiking neurons during memory encoding. Clusters of spiking neurons were identified using the DBSCAN clustering algorithm (see Materials and methods: clustering of spiking neurons and intersection over union for details). In networks with 0% inhibitory neurons, the stimulation-induced spread of activity ( $A_{leak}$ ) exceeded the trained region ( $A_{train}$ ) due to unregulated excitatory input increasing the firing probability of postsynaptic neurons. As the proportion of inhibitory neurons increased,  $A_{leak}$  became confined to  $A_{train}$ , forming a clearer boundary of the embedded image. Scale bar: 200  $\mu\text{m}$ . **(B)** Maps of spiking neurons during memory recall in response to partial cue (small circle within the trained region). Networks with 0% inhibitory neurons exhibited uncontrolled propagation of spiking activity from the cue site, indicating imprecise memory recall. At 100% inhibition, activity was limited to the cue site with no propagation, reflecting recall failure. In contrast, networks with 20% inhibitory neurons showed more localized and accurate recall of the trained image. Scale bar: 200  $\mu\text{m}$ . **(C)** Spike rates during recall for networks with 0, 20, and 100% inhibitory neurons. Networks composed entirely of excitatory neurons (0%) showed the highest spike rates due to lack of inhibitory control. Conversely, networks with all inhibitory neurons (100%) showed minimal activity. Networks with 20% inhibition achieved moderate but targeted firing, consistent with effective recall. **(D)** Intersection over union (IoU) values between  $A_{leak}$  and  $A_{train}$  across inhibitory neuron ratios during encoding and recall ( $n = 4$ ). At 0%, the lowest IoU during encoding reflected poor memory formation, which resulted in poor recall. Introducing inhibitory neurons improved IoUs, with the highest encoding IoU at 100%, but this dropped by 93% during recall, indicating over-suppression. Optimal memory retrieval occurred at 20% inhibition, where recall IoU was highest. Although recall IoU was 21% lower than encoding IoU at this ratio, the difference was not statistically significant.

increase in spike rate, limited to the immediate cue region. The 20% condition showed an intermediate but structured spike rate response, consistent with controlled and targeted recall.

To quantify memory fidelity, we computed IoU between  $A_{train}$  and  $A_{leak}$  (Figure 6D). Statistical analysis revealed significant effects of inhibitory ratio ( $F_{5, 36} = 20.29$ ,  $p < 0.001$ ), phase (encoding

vs. recall;  $F_{1, 36} = 1,194.73$ ,  $p < 0.001$ ), and their interaction ( $F_{5, 36} = 37.45$ ,  $p < 0.001$ ). Overall, IoUs during encoding were significantly higher than during recall ( $p < 0.001$ ), reflecting the probabilistic nature of recall, i.e., retrieval does not perfectly reproduce the original activation pattern on every trial.

During encoding, the 0% inhibitory condition yielded the lowest IoU, indicating the poorest encoding quality. IoU increased with higher inhibitory neuron ratios, reflecting more spatially confined memory formation. During recall, the lowest IoU (0.1748) was observed in the 0% condition, due to poor encoding and uncontrolled spread of activity. In the 100% inhibitory case, the IoU difference between encoding and recall was largest, decreasing by 93% ( $p < 0.001$ ) suggesting strong encoding but near-total failure of recall.

The optimal recall performance occurred at a 20% inhibitory neuron ratio, which yielded the highest recall IoU. At this ratio, the recall IoU was only 21% lower than the encoding IoU (0.7900-fold), and the difference was not statistically significant ( $p = 0.0586$ ), indicating that the network was able to recall approximately 79% of the actual image embedded during training. This result is consistent with prior works showing that a balanced interplay between excitation and inhibition is critical for stabilizing network activity and regulating sensory-evoked responses (Isaacson and Scanziani, 2011; Vogels et al., 2011). In the context of our study, the absence of inhibition can lead to runaway excitation and poor memory recall regardless of changes in tension. This suggests that sufficient inhibition provides a necessary stabilizing condition under which tension-driven increases in vesicle availability and synaptic efficacy can support precise memory encoding and accurate recall, rather than producing uncontrolled network activity.

## Tension enhances projection between assemblies

Projection, an advanced cognitive operation, refers to the activation of a downstream assembly (B) by an upstream assembly (A), effectively “projecting” learned information across regions. To model this process, we trained two spatially separated assemblies within the network (Figure 7A). During training, region A (square) received full stimulation, while region B (triangle) was partially stimulated 2 ms later (40% of neurons), to encourage directed connectivity from A to B without forming an independent assembly in B.

During training, most neurons in region A responded and fired in response to stimulation, whereas a smaller subset of neurons in B fired with a 2 ms delay due to the weaker, delayed input (Figure 7B). After training, activation of region A alone was sufficient to trigger delayed firing in region B, indicating successful projection from A to B. In contrast, no such projection was observed in the untrained network, where activity in A failed to elicit any response in B. This dynamic propagation is visualized in [Supplementary Video S2](#).

Spike rate profiles further support this observation. In the trained network, activation of A led to a spike rate surge in region B with a consistent short delay (~2 ms). No changes were observed in an unrelated control region (C), confirming that projection was specific to the A→B connection. In the untrained network,

spike rates in A were lower, reflecting weaker intra-assembly connections, and no activity was detected in B, confirming the absence of projection.

To quantify projection strength, we computed the synchrony index between assemblies A and B (see Materials and methods: synchrony index between two assemblies for details). Mechanical tension significantly modulated projection efficacy (one-way ANOVA  $F_{4, 15} = 19.74$ ,  $p < 0.001$ ; Figure 7C). Increasing tension from the resting level (100–150%) enhanced the synchrony index by 7% relative to baseline ( $p = 0.0134$ ), suggesting that tension facilitates inter-assembly communication. Conversely, reducing tension to 50% of resting levels led to an 8% decrease in synchrony ( $p = 0.0044$ ), likely due to decreased vesicle availability and impaired synaptic transmission. Together, these results suggest that mechanical tension not only affects individual neuron firing but also governs the functional coupling between assemblies necessary for information flow.

## Tension and training duration modulate associative memory recall

We investigated associative memory, a higher-order cognitive function involving the functional linking of distinct neural assemblies. To model this process, we simultaneously trained two spatially separated rectangular regions (see Materials and methods: *in silico* stimulation for details). To test associative recall, we applied a partial cue by stimulating only the right rectangular region and monitored activity in the unstimulated left region (Figure 8A). We also manipulated mechanical tension to examine its influence on memory accessibility.

During training, neurons across both regions exhibited temporally coordinated spiking, reflecting their joint activation by the composite stimulation pattern (Figure 8C). In the recall phase, stimulation of the right region alone evoked synchronous bursts not only locally but also in the left region, indicating functional linkage and associative memory recall. In contrast, when the same cue was applied to an untrained network, only spontaneous, uncoordinated activity appeared in the left region, indicating no stored association.

We quantified recall performance using the synchrony index between the two assemblies (see Materials and methods: synchrony index between two assemblies for details; Figure 8B). A repeated-measures two-way ANOVA revealed significant effects of recall time ( $F_{4, 36} = 5.84$ ,  $p < 0.001$ ), training duration ( $F_{2, 9} = 131.23$ ,  $p < 0.001$ ), and their interaction ( $F_{8, 36} = 4.87$ ,  $p < 0.001$ ). The trained networks exhibited high synchrony during training, driven by co-stimulation, and maintained elevated synchrony during recall compared to untrained controls ( $p < 0.001$ ). However, synchrony declined gradually over 25 s of recall, indicating memory decay. Networks trained for 2 s showed significantly higher synchrony than those trained for 1 s ( $p = 0.0034$ ), suggesting that longer training enhances both strength and longevity of memory associations.

Lastly, to test whether mechanical tension qualitatively regulates memory accessibility and reversibility, we focused on three biologically interpretable tension regimes: relaxed,

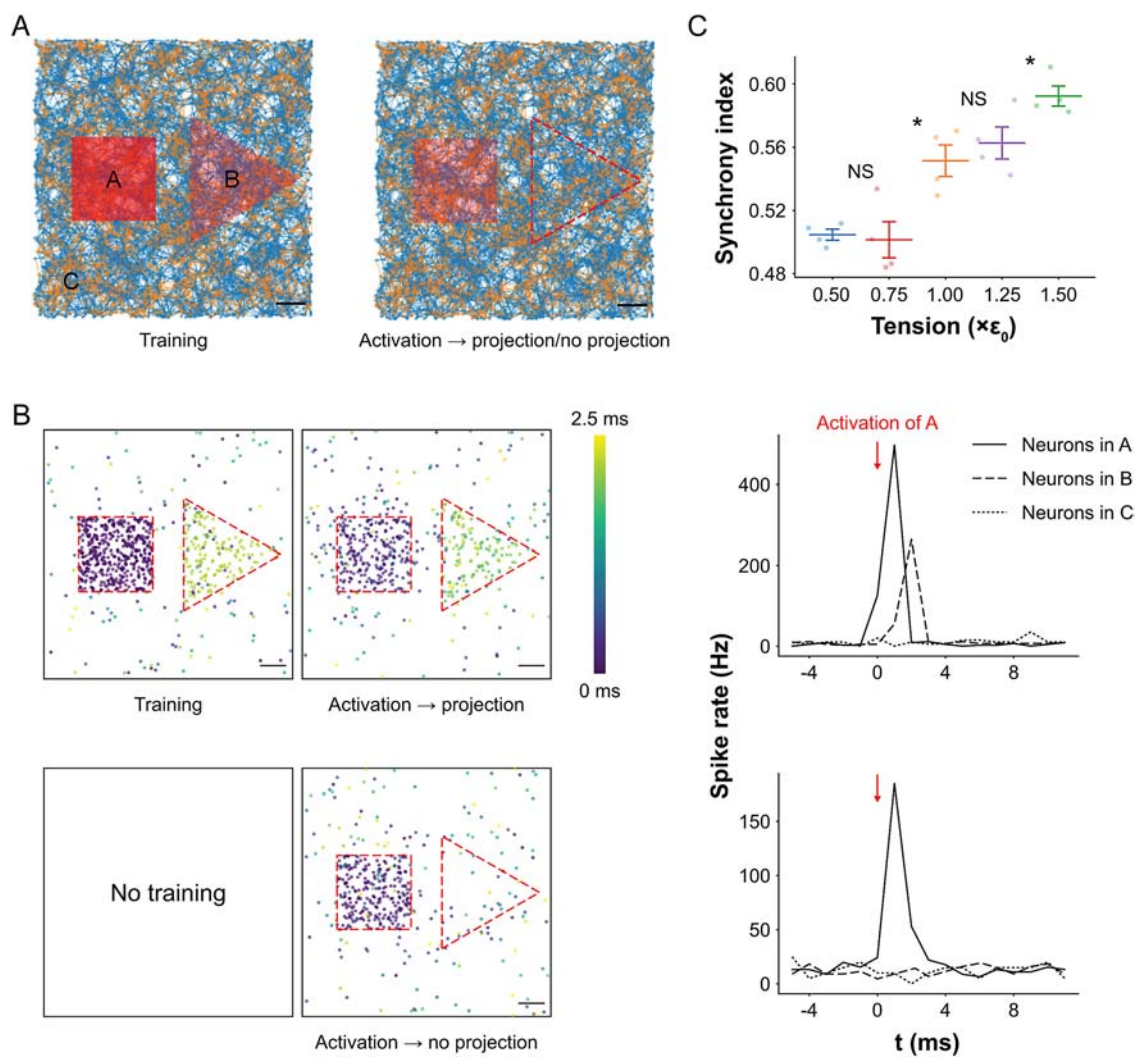


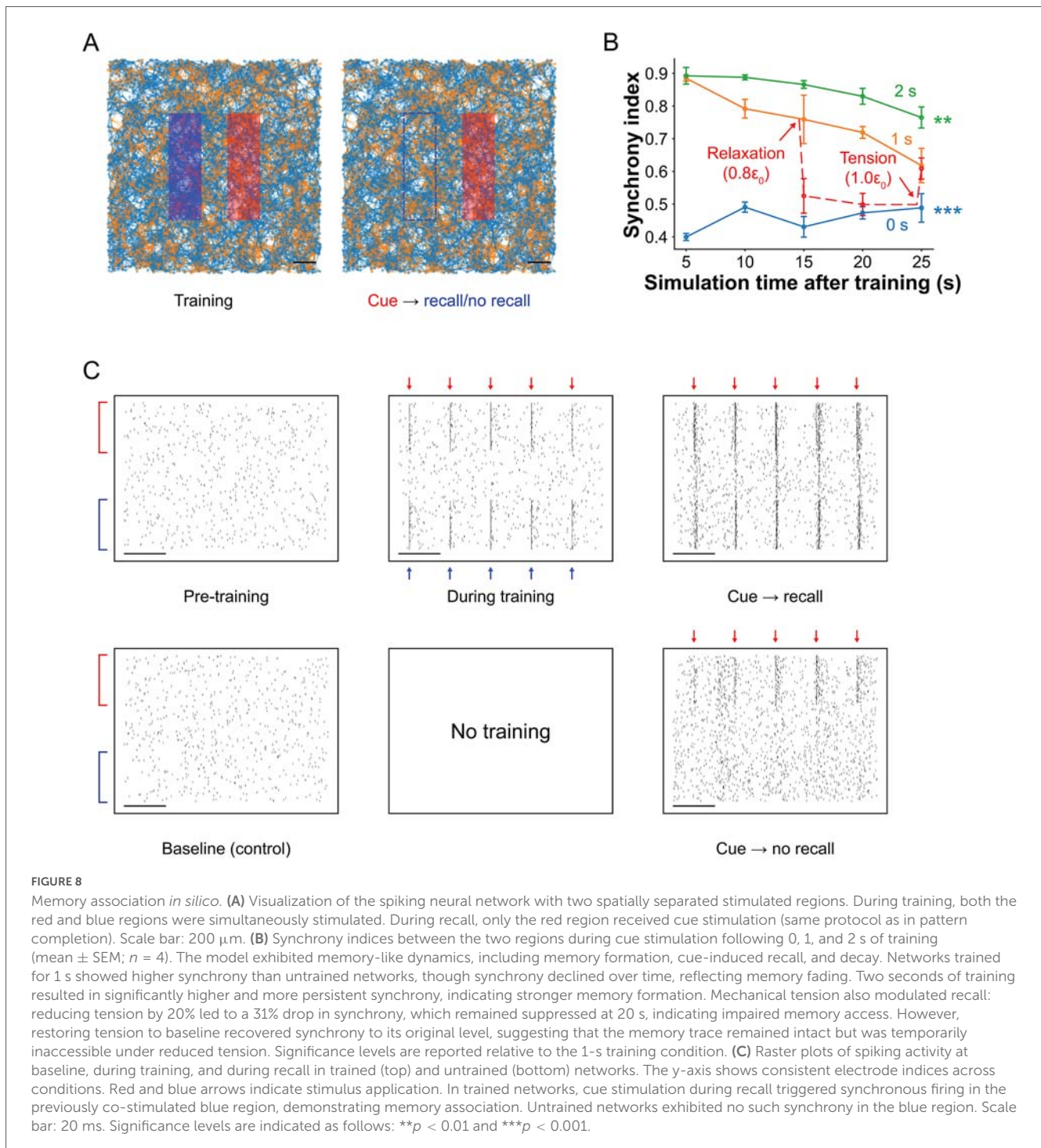
FIGURE 7

Projection between neural assemblies *in silico*. (A) Visualization of neural networks during training and projection. The transparency of stimulated regions represents relative stimulation intensity. During training, neurons in region A were fully stimulated (same protocol as in pattern completion) to form a neural assembly. Neurons in region B were stimulated 2 ms after region A and at 40% of A's stimulation intensity to encourage the formation of connectivity from A to B without creating an independent assembly in B. Scale bar: 200  $\mu\text{m}$ . (B) Maps of spiking neurons within a 2.5 ms window after activation of region A during projection, comparing trained (top left) and untrained (bottom left) networks. Corresponding spike rates in regions A, B, and C are shown during projection for trained (top right) and untrained (bottom right) conditions. In the trained network, neurons in region A responded strongly during training, while region B showed delayed and weaker activation due to partial stimulation. During projection, activation of A induced activity in B with a short lag, indicating successful projection. Region C exhibited no activity, confirming that it is not involved in the projection. In contrast, the untrained network showed no projection from A to B, as reflected by the absence of spiking activity in B. Scale bar: 200  $\mu\text{m}$ . (C) Synchrony indices between assemblies A and B under different tension levels (mean  $\pm$  SEM;  $n = 4$ ). Higher tension (150% of baseline, i.e.,  $1.5\epsilon_0$ ) significantly increased synchrony by 7%, while lower tension (50% of baseline, i.e.,  $0.5\epsilon_0$ ) decreased synchrony by 8%, relative to the resting tension ( $1.0\epsilon_0$ ). These results indicate that mechanical tension enhances projection between neural assemblies. Significance levels are shown between two tension levels. Significance levels are indicated as follows: not significant (ns) and  $*p < 0.05$ .

baseline, and elevated. Following 1 s of training, network tension was reduced by 20%, resulting in a 31% decrease in the synchrony index ( $p = 0.0423$ ), which remained significantly suppressed after 20 s ( $p = 0.0012$ ). Crucially, restoring tension to baseline fully recovered synchrony levels ( $p = 0.8863$ ), indicating reinstatement of associative recall. These findings suggest that memory was not erased during relaxation but rendered temporarily inaccessible, likely due to reduced vesicle availability and impaired synaptic efficacy. Restoring tension reinstated effective synaptic transmission and re-enabled memory retrieval.

## Discussion

In this study, we developed an *in silico* platform to investigate how the mechanical tensional state of neural networks modulates high-level cognitive operations, including learning, memory, projection, and association. While recent studies have shown that mechanical tension can influence axonal outgrowth, synaptic plasticity, vesicle accumulation, and neural excitability (Dennerll et al., 1989; Pfister et al., 2004; Siechen et al., 2009; Ahmed et al., 2012; Fan et al., 2015; Falconieri et al., 2023; Joy et al., 2023; Lee et al., 2023), our work advances this line



of research by integrating tension directly into a biologically inspired spiking neural network model. The model predicts that increased tension enhances synaptic function by promoting vesicle clustering at presynaptic terminals and accelerating vesicle replenishment. Mechanistically, faster replenishment of releasable vesicles increases the likelihood that closely timed presynaptic spikes evoke effective postsynaptic responses, thereby promoting coincident activation within trained assemblies. This provides a plausible causal link between experimentally observed tension-dependent vesicle accumulation and the enhanced assembly

synchrony and recall speed observed in our simulations. These tension-driven improvements in synaptic dynamics translate into faster memory recall, stronger neural synchrony, and more reliable execution of cognitive operations, suggesting that mechanical tension may serve as a key modulator in both biological and artificial neural systems.

We modeled learning-based plasticity using STDP, allowing synaptic weights to adapt based on the temporal order of pre- and postsynaptic spikes. This mechanism enabled the network to encode and recall learned information. However, to more faithfully

capture the dynamics of brain activity, future models should incorporate neural bursting. Bursting, defined as consecutive spikes recorded from a single electrode *in vivo* or *in vitro*, has been linked to memory-related processes and can arise from multiple mechanisms, including the spatial organization of synaptic inputs (Larkum et al., 1999), ionic dynamics involving voltage-gated calcium channels (Cain and Snutch, 2010), and modulation of  $\text{Ca}^{2+}$  conductance via G protein-coupled receptors such as metabotropic glutamate receptors (mGluRs) (Hildebrand et al., 2009). In humans, ripple oscillations, transient high-frequency bursts exceeding 80 Hz, are thought to support memory encoding and recall (Jadhav et al., 2012; Buzsáki, 2015; Norman et al., 2019; Staresina et al., 2023). However, our computational model did not reproduce bursts at the single-neuron level. Given the functional significance of bursting in cognitive operations, future models should incorporate burst-generating mechanisms to more accurately capture how mechanical tension may shape biologically realistic patterns of memory and learning.

Beyond bursting dynamics, neural assemblies are known to engage in a variety of activity patterns and plasticity mechanisms that support memory formation and consolidation, particularly during offline states. Although the present study focuses on online learning and short-term memory encoding, rather than long-term memory consolidation, these additional mechanisms represent important directions for future investigation under mechanical tension.

In particular, slow oscillations during sleep (Rasch and Born, 2013), together with spindles and ripple events (Staresina et al., 2023), are thought to coordinate the reactivation, redistribution, and stabilization of memory traces across brain regions and to drive synaptic modification during offline consolidation. Likewise, biologically motivated multi-phase synaptic plasticity mechanisms such as synaptic-tagging-and-capture (STC) enable transient synaptic changes to be stabilized into long-term memory. In STC, weakly activated synapses during learning are “tagged” and can later capture plasticity-related proteins synthesized in response to strong activation elsewhere in the network, thereby converting into long-lasting synaptic modifications (Frey and Morris, 1997). These processes may support post-learning improvements in memory accuracy without additional external input (Luboevski and Tetzlaff, 2021). Incorporating such offline dynamics and multi-phase plasticity into future models would allow investigation of how mechanical tension interacts with memory consolidation and long-term stabilization of neural assemblies.

A key insight from our model was the essential role of inhibitory neurons in memory encoding and recall, as sufficient inhibition prevents tension-driven enhancements of vesicle dynamics from being overwhelmed by unbounded excitatory activity. In networks lacking inhibition (0% inhibitory neurons), memory encoding was poor due to the unbounded excitatory activity of presynaptic neurons, and cue stimulation triggered uncontrolled propagation of spikes far beyond the trained region. This is consistent with the well-established role of inhibition in maintaining network stability and regulating sensory-evoked responses (Isaacson and Scanziani, 2011; Vogels et al., 2011). Conversely, in networks composed entirely of inhibitory neurons (100%), we observed the formation of clearly defined memory traces during training due to suppressed firing at the boundary of the trained region but during recall, activity remained strictly

confined to the cue site and failed to propagate, resulting in poor memory retrieval. The optimal encoding and recall occurred at an intermediate configuration, approximately 20% inhibitory neurons, where excitation was sufficiently constrained to allow precise and localized memory recall. Mechanistically, the optimal number of inhibitory neurons counterbalance tension-amplified excitatory drive by stabilizing membrane potentials and limiting excessive recruitment of untrained neurons. In this way, inhibition enables tension to selectively enhance trained assemblies rather than globally increasing network activity. This result is broadly consistent with anatomical data: in mice and rats, 7–11% of hippocampal neurons are GABAergic interneurons (inhibitory), with the remainder being excitatory (Gulyás et al., 1999; Bezaire and Soltesz, 2013). In primates, GABAergic neurons constitute approximately 20–25% of cortical neurons (Hendry et al., 1987; DeFelipe et al., 2002). Together, these findings reinforce the idea that inhibitory neurons are not merely suppressive but play a critical regulatory role, refining and stabilizing neural representations to support accurate memory encoding and recall while preventing pathological excitation and network instability.

Our findings on assembly activities such as pattern completion, projection, and association invite a deeper reinterpretation of assembly calculus in biological terms. Assembly calculus conceptualizes neural assemblies as symbolic representations of concepts such as images or words, and models cognitive operations using abstract logical rules (e.g., “if A fires, then B fires”) (Papadimitriou et al., 2020). However, our work demonstrates that such high-level operations can emerge from low-level, biologically plausible mechanisms, including STDP and vesicle dynamics. Notably, we observed that the success of projection and association was modulated by mechanical tension, suggesting the presence of a neuromechanical layer in cognitive control.

This raises the possibility that tension acts not only as a modulator of firing and plasticity, but as a control mechanism, determining when, where and under what conditions assemblies can interact with each other. In this view, mechanical forces impose real-world, physical constraints on otherwise abstract symbolic operations, effectively bridging the gap between continuous biological dynamics and discrete computational logic. Taken together, our results suggest that high-level cognitive functions may emerge not solely from fixed logical architectures, but from the interplay of structural connectivity, plasticity, and physical state, pointing toward a more integrated and dynamic model of cognition.

Another compelling implication of our model lies in its potential relevance to clinical memory disorders such as Alzheimer’s disease, dementia, and amnesia. In our simulations, relaxing mechanical tension in the network led to a significant drop in the synchrony index, indicating impaired memory recall. However, when tension was restored to its original level, synchrony returned to baseline suggesting that the memory trace itself had not been erased, but had become temporarily inaccessible under low-tension conditions. This finding aligns with prevailing hypotheses in clinical neuroscience, which propose that patients with memory impairments may not suffer from the loss of stored memories, but rather from disrupted access to intact memory traces (Roy et al., 2016; De Simone et al., 2020).

Mechanistically, our model offers a plausible explanation: reduced tension leads to diminished vesicle clustering and slower vesicle replenishment, impairing synaptic transmission and preventing the network from reactivating previously learned assemblies, without compromising synaptic efficacy that was acquired through synaptic plasticity. When tension is reinstated, vesicle availability is restored, allowing memory recall to resume due to synaptic efficacy acquired during learning before reduction of tension. These results suggest that the mechanical state of neural tissue may play a direct and reversible role in determining whether memories can be accessed, rather than whether they are stored at all, providing a new interpretive lens for memory systems.

In summary, we demonstrated that mechanical tension enhances key cognitive operations, including pattern completion, projection, learning, and memory, within a biologically inspired spiking neural network model. These findings provide a conceptual foundation for the development of biocompatible or biohybrid computing systems that exploit physical principles such as tension for learning and memory. More broadly, they advance our understanding of mechanical tension as an active neuromodulatory factor in cognitive function. Future work can build on this framework to investigate how mechanical states influence other brain functions, including computation, reasoning, planning, language, and forgetting, opening new directions across neuroscience, artificial intelligence, and neuroengineering.

## Data availability statement

The raw data supporting the conclusions of this article will be made available by the authors, without undue reservation.

## Author contributions

KL: Writing – original draft, Writing – review & editing. MS: Writing – review & editing.

## Funding

The author(s) declared that financial support was received for this work and/or its publication. This work was supported by the National Science Foundation Expedition project, “Mind *in vitro*—Computing with Living Neurons” (2123781), the National Aeronautics and Space Administration (00759340), the National Science Foundation CMMI (23-42257), and the Chan Zuckerberg Biohub Investigator grant.

## References

- Ahmed, W. W., Li, T. C., Rubakhin, S. S., Chiba, A., Sweedler, J. V., and Saif, T. A. (2012). Mechanical tension modulates local and global vesicle dynamics in neurons. *Cell Mol. Bioeng.* 5, 155–164. doi: 10.1007/s12195-012-0223-1
- Arikath, J. (2010). N-cadherin: stabilizing synapses. *J. Cell. Biol.* 189, 397–398. doi: 10.1083/jcb.201004022
- Attneave, F. B. M., and Hebb, D. O. (1950). The organization of behavior; a neuropsychological theory. *Am. J. Psychol.* 63:378. doi: 10.2307/1418888
- Bertram, R., Sherman, A., and Stanley, E. F. (1996). Single-domain/bound calcium hypothesis of transmitter release and facilitation. *J. Neurophysiol.* 75, 1919–1931. doi: 10.1152/jn.1996.75.5.1919

## Conflict of interest

The author(s) declared that this work was conducted in the absence of any commercial or financial relationships that could be construed as a potential conflict of interest.

## Generative AI statement

The author(s) declared that generative AI was not used in the creation of this manuscript.

Any alternative text (alt text) provided alongside figures in this article has been generated by Frontiers with the support of artificial intelligence and reasonable efforts have been made to ensure accuracy, including review by the authors wherever possible. If you identify any issues, please contact us.

## Publisher’s note

All claims expressed in this article are solely those of the authors and do not necessarily represent those of their affiliated organizations, or those of the publisher, the editors and the reviewers. Any product that may be evaluated in this article, or claim that may be made by its manufacturer, is not guaranteed or endorsed by the publisher.

## Supplementary material

The Supplementary Material for this article can be found online at: <https://www.frontiersin.org/articles/10.3389/fncom.2026.1737434/full#supplementary-material>

### SUPPLEMENTARY VIDEO S1

Pattern completion with and without training. Spatiotemporal propagation of spiking activity upon cue stimulation in trained (left) and untrained (right) networks. In the trained network, spiking initiated at the cue sites rapidly propagates across the trained region, demonstrating successful pattern completion. In contrast, the untrained network shows restricted activity confined to the cue sites, with no propagation. Each frame represents neural activity within a 1 ms time window. Total duration: 15 ms. Scale bar: 200  $\mu$  m.

### SUPPLEMENTARY VIDEO S2

Projection with and without training. Spatiotemporal propagation of spiking activity following activation of assembly A in trained (left) and untrained (right) networks. In the trained network, activation of A successfully triggers projection to assembly B with a short temporal lag. In contrast, the untrained network shows no projection from A to B. Each frame represents neural activity within a 1 ms time window. Total duration: 15 ms. Scale bar: 200  $\mu$  m.

- Bezire, M. J., and Soltesz, I. (2013). Quantitative assessment of CA1 local circuits: knowledge base for interneuron-pyramidal cell connectivity. *Hippocampus* 23, 751–785. doi: 10.1002/hipo.22141
- Bi, G. Q., and Poo, M. M. (1998). Synaptic modifications in cultured hippocampal neurons: dependence on spike timing, synaptic strength, and postsynaptic cell type. *J. Neurosci.* 18, 10464–10472. doi: 10.1523/JNEUROSCI.18-24-10464.1998
- Bliss, T. V., and Collingridge, G. L. (1993). A synaptic model of memory: long-term potentiation in the hippocampus. *Nature* 361, 31–39. doi: 10.1038/361031a0
- Bray, D. (1979). Mechanical tension produced by nerve cells in tissue culture. *J. Cell. Sci.* 37, 391–410. doi: 10.1242/jcs.37.1.391
- Brunel, N. (2000). Dynamics of sparsely connected networks of excitatory and inhibitory spiking neurons. *J. Comput. Neurosci.* 8, 183–208. doi: 10.1023/a:1008925309027
- Buzsáki, G. (2015). Hippocampal sharp wave-ripple: a cognitive biomarker for episodic memory and planning. *Hippocampus* 25, 1073–1188. doi: 10.1002/hipo.22488
- Cain, S. M., and Snutch, T. P. (2010). Contributions of T-type calcium channel isoforms to neuronal firing. *Channels* 4, 475–482. doi: 10.4161/chan.4.6.14106
- Calderwood, D. A., Campbell, I. D., and Critchley, D. R. (2013). Talins and kindlins: partners in integrin-mediated adhesion. *Nat. Rev. Mol. Cell Biol.* 14, 503–517. doi: 10.1038/nrm3624
- De Simone, M. S., De Tollis, M., Fadda, L., Perri, R., Caltagirone, C., and Carlesimo, G. A. (2020). Lost or unavailable? Exploring mechanisms that affect retrograde memory in mild cognitive impairment and Alzheimer's disease patients. *J. Neurol.* 267, 113–124. doi: 10.1007/s00415-019-09559-8
- DeFelipe, J., Alonso-Nanclares, L., and Arellano, J. I. (2002). Microstructure of the neocortex: comparative aspects. *J. Neurocytol.* 31, 299–316. doi: 10.1023/a:1024130211265
- Dennerll, T. J., Lamoureux, P., Buxbaum, R. E., and Heidemann, S. R. (1989). The cytomechanics of axonal elongation and retraction. *J. Cell. Biol.* 109(6 Pt 1), 3073–3083. doi: 10.1083/jcb.109.6.3073
- Ester, M., Kriegl, H. P., Sander, J., and Xu, X. (1996). “A density-based algorithm for discovering clusters a density-based algorithm for discovering clusters in large spatial databases with noise,” in *Proceedings - 2nd International Conference on Knowledge Discovery and Data Mining, KDD*, (Portland).
- Falconieri, A., De Vincentiis, S., Cappello, V., Convertino, D., Das, R., Ghignoli, S., et al. (2023). Axonal plasticity in response to active forces generated through magnetic nano-pulling. *Cell Rep.* 42:111912. doi: 10.1016/j.celrep.2022.111912
- Fan, A., Stebbings, K. A., Llano, D. A., and Saif, T. (2015). Stretch induced hyperexcitability of mice callosal pathway. *Front. Cell Neurosci.* 9:292. doi: 10.3389/fncel.2015.00292
- Feldman, D. E. (2000). Timing-based LTP and LTD at vertical inputs to layer II/III pyramidal cells in rat barrel cortex. *Neuron* 27, 45–56. doi: 10.1016/s0896-6273(00)00008-8
- Frey, U., and Morris, R. G. (1997). Synaptic tagging and long-term potentiation. *Nature* 385, 533–536. doi: 10.1038/385533a0
- Furcila, D., Domínguez-Álvarez, M., DeFelipe, J., and Alonso-Nanclares, L. (2019). Subregional density of neurons, neurofibrillary tangles and amyloid plaques in the hippocampus of patients with Alzheimer's Disease. *Front. Neuroanat.* 13:99. doi: 10.3389/fnana.2019.00099
- Gerstein, G. L., Bedenbaugh, P., and Aertens, M. H. (1989). Neuronal assemblies. *IEEE Trans. Biomed. Eng.* 36, 4–14. doi: 10.1109/10.16444
- Gerstner, W., Kistler, W. M., Naud, R., and Paninski, L. (2014). *Neuronal Dynamics: From Single Neurons to Networks and Models of Cognition*. Cambridge: Cambridge University Press. doi: 10.1017/CBO9781107447615
- Gillies, S., van der Wel, C., Van den Bossche, J., Taves, M. W., Arnott, J., Ward, B. C., et al. (2022). *Shapely*. Geneva: Zenodo. doi: 10.5281/ZENODO.7428463
- Gulyás, A. I., Megias, M., Emri, Z., and Freund, T. F. (1999). Total number and ratio of excitatory and inhibitory synapses converging onto single interneurons of different types in the CA1 area of the rat hippocampus. *J. Neurosci.* 19, 10082–10097. doi: 10.1523/JNEUROSCI.19-22-10082.1999
- Hendry, S. H., Schwark, H. D., Jones, E. G., and Yan, J. (1987). Numbers and proportions of GABA-immunoreactive neurons in different areas of monkey cerebral cortex. *J. Neurosci.* 7, 1503–1519. doi: 10.1523/JNEUROSCI.07-05-01503.1987
- Hildebrand, M. E., Isope, P., Miyazaki, T., Nakaya, T., Garcia, E., Feltz, A., et al. (2009). Functional coupling between mGluR1 and Cav3.1 T-type calcium channels contributes to parallel fiber-induced fast calcium signaling within Purkinje cell dendritic spines. *J. Neurosci.* 29, 9668–9682. doi: 10.1523/JNEUROSCI.0362-09.2009
- Isaacson, J. S., and Scanziani, M. (2011). How inhibition shapes cortical activity. *Neuron* 72, 231–243. doi: 10.1016/j.neuron.2011.09.027
- Jadhav, S. P., Kemere, C., German, P. W., and Frank, L. M. (2012). Awake hippocampal sharp-wave ripples support spatial memory. *Science* 336, 1454–1458. doi: 10.1126/science.1217230
- Joy, M. S. H., Nall, D. L., Emon, B., Lee, K. Y., Barishman, A., Ahmed, M., et al. (2023). Synapses without tension fail to fire in an in vitro network of hippocampal neurons. *Proc. Natl. Acad. Sci. U. S. A.* 120:e2311995120. doi: 10.1073/pnas.2311995120
- Kandel, E., Schwartz, J., Jessell, T., Siegelbaum, S., and Hudspeth, A. (2012). *Principle of Neural Science*, 5th Edn. Columbus, OH: McGraw-Hill.
- Kavalali, E. T. (2015). The mechanisms and functions of spontaneous neurotransmitter release. *Nat. Rev. Neurosci.* 16, 5–16. doi: 10.1038/nrn3875
- Kriener, B., Enger, H., Tetzlaff, T., Plesser, H. E., Gewaltig, M. O., and Einevoll, G. T. (2014). Dynamics of self-sustained asynchronous-irregular activity in random networks of spiking neurons with strong synapses. *Front. Comput. Neurosci.* 8:136. doi: 10.3389/fncom.2014.00136
- Langille, J. J., and Brown, R. E. (2018). The synaptic theory of memory: a historical survey and reconciliation of recent opposition. *Front. Syst. Neurosci.* 12:52. doi: 10.3389/fnsys.2018.00052
- Larkum, M. E., Zhu, J. J., and Sakmann, B. (1999). A new cellular mechanism for coupling inputs arriving at different cortical layers. *Nature* 398, 338–341. doi: 10.1038/18686
- Leckband, D. E., and de Rooij, J. (2014). Cadherin adhesion and mechanotransduction. *Annu. Rev. Cell. Dev. Biol.* 30, 291–315. doi: 10.1146/annurev-cellbio-100913-013212
- Lee, K. Y., Rhodes, J. S., and Saif, M. T. A. (2023). Astrocyte-mediated transduction of muscle fiber contractions synchronizes hippocampal neuronal network development. *Neuroscience* 515, 25–36. doi: 10.1016/j.neuroscience.2023.01.028
- Luboevski, J., and Tetzlaff, C. (2021). Memory consolidation and improvement by synaptic tagging and capture in recurrent neural networks. *Commun. Biol.* 4:275. doi: 10.1038/s42003-021-01778-y
- Magee, J. C., and Johnston, D. (1997). A synaptically controlled, associative signal for Hebbian plasticity in hippocampal neurons. *Science* 275, 209–213. doi: 10.1126/science.275.5297.209
- Markram, H., Lübke, J., Frotscher, M., and Sakmann, B. (1997). Regulation of synaptic efficacy by coincidence of postsynaptic APs and EPSPs. *Science* 275, 213–215. doi: 10.1126/science.275.5297.213
- Morrison, A., Diesmann, M., and Gerstner, W. (2008). Phenomenological models of synaptic plasticity based on spike timing. *Biol. Cybern.* 98, 459–478. doi: 10.1007/s00422-008-0233-1
- Norman, Y., Yeagle, E. M., Khuvis, S., Harel, M., Mehta, A. D., and Malach, R. (2019). Hippocampal sharp-wave ripples linked to visual episodic recollection in humans. *Science* 365:eaax1030. doi: 10.1126/science.aax1030
- Oja, E. (1982). A simplified neuron model as a principal component analyzer. *J. Math. Biol.* 15, 267–273. doi: 10.1007/BF00275687
- O'Leary, J. D., Bruckner, R., Autore, L., and Ryan, T. J. (2024). Natural forgetting reversibly modulates engram expression. *Elife* 12:R92860. doi: 10.7554/eLife.92860
- Papadimitriou, C. H., Vempala, S. S., Mitropolsky, D., Collins, M., and Maass, W. (2020). Brain computation by assemblies of neurons. *Proc. Natl. Acad. Sci. U. S. A.* 117, 14464–14472. doi: 10.1073/pnas.2001893117
- Pfister, B. J., Iwata, A., Meaney, D. F., and Smith, D. H. (2004). Extreme stretch growth of integrated axons. *J. Neurosci.* 24, 7978–7983. doi: 10.1523/JNEUROSCI.1974-04.2004
- Pozo, K., Cingolani, L. A., Bassani, S., Laurent, F., Passafaro, M., and Goda, Y. (2012).  $\beta 3$  integrin interacts directly with GluA2 AMPA receptor subunit and regulates AMPA receptor expression in hippocampal neurons. *Proc. Natl. Acad. Sci. U. S. A.* 109, 1323–1328. doi: 10.1073/pnas.1113736109
- Rasch, B., and Born, J. (2013). About sleep's role in memory. *Physiol. Rev.* 93, 681–766. doi: 10.1152/physrev.00032.2012
- Roy, D. S., Arons, A., Mitchell, T. I., Pignatelli, M., Ryan, T. J., and Tonegawa, S. (2016). Memory retrieval by activating engram cells in mouse models of early Alzheimer's disease. *Nature* 531, 508–512. doi: 10.1038/nature17172
- Ryan, T. J., and Frankland, P. W. (2022). Forgetting as a form of adaptive engram cell plasticity. *Nat. Rev. Neurosci.* 23, 173–186. doi: 10.1038/s41583-021-00548-3
- Siechen, S., Yang, S., Chiba, A., and Saif, T. (2009). Mechanical tension contributes to clustering of neurotransmitter vesicles at presynaptic terminals. *Proc. Natl. Acad. Sci. U. S. A.* 106, 12611–12616. doi: 10.1073/pnas.0901867106
- Song, S., Miller, K. D., and Abbott, L. F. (2000). Competitive Hebbian learning through spike-timing-dependent synaptic plasticity. *Nat. Neurosci.* 3, 919–926. doi: 10.1038/78829
- Staresina, B. P., Niediek, J., Borger, V., Surges, R., and Mormann, F. (2023). How coupled slow oscillations, spindles and ripples coordinate neuronal processing and communication during human sleep. *Nat. Neurosci.* 26, 1429–1437. doi: 10.1038/s41593-023-01381-w
- Stimberg, M., Brette, R., and Goodman, D. F. (2019). Brian 2, an intuitive and efficient neural simulator. *Elife* 8:e47314. doi: 10.7554/eLife.47314

- Takeichi, M. (2007). The cadherin superfamily in neuronal connections and interactions. *Nat. Rev. Neurosci.* 8, 11–20. doi: 10.1038/nrn2043
- Thalhammer, A., and Cingolani, L. A. (2014). Cell adhesion and homeostatic synaptic plasticity. *Neuropharmacology* 78, 23–30. doi: 10.1016/j.neuropharm.2013.03.015
- Tofangchi, A., Fan, A., and Saif, M. T. A. (2016). Mechanism of axonal contractility in embryonic drosophila motor neurons in vivo. *Biophys. J.* 111, 1519–1527. doi: 10.1016/j.bpj.2016.08.024
- Tsodyks, M., Pawelzik, K., and Markram, H. (1998). Neural networks with dynamic synapses. *Neural Comput.* 10, 821–835. doi: 10.1162/089976698300017502
- Vallat, R. (2018). Pingouin: statistics in Python. *J. Open Source Softw.* 3:1026. doi: 10.21105/joss.01026
- van Vreeswijk, C., and Sompolinsky, H. (1996). Chaos in neuronal networks with balanced excitatory and inhibitory activity. *Science* 274, 1724–1726. doi: 10.1126/science.274.5293.1724
- Vogel, V., and Sheetz, M. (2006). Local force and geometry sensing regulate cell functions. *Nat. Rev. Mol. Cell Biol.* 7, 265–275. doi: 10.1038/nrm1890
- Vogels, T. P., Sprekeler, H., Zenke, F., Clopath, C., and Gerstner, W. (2011). Inhibitory plasticity balances excitation and inhibition in sensory pathways and memory networks. *Science* 334, 1569–1573. doi: 10.1126/science.1211095
- Warren, M. S., Bradley, W. D., Gourley, S. L., Lin, Y. C., Simpson, M. A., Reichardt, L. F., et al. (2012). Integrin  $\beta 1$  signals through Arg to regulate postnatal dendritic arborization, synapse density, and behavior. *J. Neurosci.* 32, 2824–2834. doi: 10.1523/JNEUROSCI.3942-11.2012